Polydisperse Adsorption: Pattern Formation Kinetics, Fractal Properties, and Transition to Order

N. V. Brilliantov[1,2], Yu. A. Andrienko[1,3], P. L. Krapivsky[4], and J. Kurths[3]
[(1)] *Moscow State University, Physics Department, Moscow 119899, Russia*
[(2)] *Department of Chemistry, University of Toronto, Toronto, Canada M5S 1A1*
[(3)] *University of Potsdam, Physics Department, Am Neuen Palais, D–14415 Potsdam, Germany*
[(4)] *Center for Polymer Studies and Department of Physics, Boston University, Boston, MA 02215*

We investigate the process of random sequential adsorption of polydisperse particles whose size distribution exhibits a power-law dependence in the small size limit, $P(R) \sim R^{\alpha-1}$. We reveal a relation between pattern formation kinetics and structural properties of arising patterns. We propose a mean-field theory which provides a fair description for sufficiently small α. When $\alpha \to \infty$, highly ordered structures locally identical to the Apollonian packing are formed. We introduce a quantitative criterion of the regularity of the pattern formation process. When $\alpha \gg 1$, a sharp transition from irregular to regular pattern formation regime is found to occur near the jamming coverage of standard random sequential adsorption with monodisperse size distribution.

PACS numbers: 81.10.Aj, 02.50.-r, 05.40.+j, 61.43.-j

I. INTRODUCTION

Random sequential adsorption (RSA) is an irreversible process in which particles are adsorbed sequentially and without overlaps and deposited particles cannot diffuse or desorb from the substrate. The RSA model has been initially applied to reactions along polymer chains [1]. More recently, RSA processes have found a variety of other applications from adhesion of colloidal particles and proteins onto substrates [2] to chemisorption [3] and epitaxial growth [4]; for reviews see [5].

In this paper, we study a simple generalization of RSA that creates a rich dynamic behavior and results in complex spatial patterns. Namely, we consider polydisperse random sequential adsorption (PRSA) processes. Adsorption of mixtures has been addressed in a very few studies [6–9]. If a mixture contains a small number of different sizes, geometric and kinetic characteristics are primarily determined by the smallest size. In many applications, however, the size distribution is continuous and spreads over several decades [10]. Therefore, before the smallest size will finally win, an interesting intermediate asymptotics arises. To address this intermediate regime, we consider PRSA with the power-law distribution in the small size limit, $P(R) \sim R^{\alpha-1}$. We show [11] that this PRSA gives rise to fractal patterns of dimension D_f depending on the exponent α. Additionally, we measure the degree of order of the patterns formed by PRSA, and identify the local structure of the patterns arising in the limit $\alpha \to \infty$ with Apollonian packing [12]. The significance of Apollonian packing in surface deposition problems was also recognized in Ref. [13].

This paper is organized as follows. In Sec. II, we introduce PRSA and present numerical results. In Sec. III, we develop scaling, exact, and mean-field approaches to PRSA. Exact results are available for the one-dimensional (1D) PRSA, and they are used to check mean-field and scaling approaches. A relation between kinetics and geometry of arising patterns is also discussed. In Sec. IV, we introduce a quantitative criterion of regularity of the pattern formation process and analyze the ordering in PRSA processes. The last Sec. V contains a summary.

II. POLYDISPERSE RSA

In applying RSA to real processes, one should take into account that adsorbed particles are typically polydisperse. The relevant example is adsorption of colloidal particles, that have a broad radii distribution. It is usually described by the Schulz distribution [14], which has a power-law dependence on the radius R for small R and an exponential tail for large R:

$$P_{Sz}(R) = \left[\frac{\alpha}{\langle R\rangle}\right]^{\alpha} \frac{R^{\alpha-1}}{\Gamma(\alpha)} \exp\left[-\frac{\alpha}{\langle R\rangle} R\right]. \qquad (1)$$

Here $\langle R\rangle$ is the average radius and $\Gamma(x)$ the gamma function. Note that the exponent α should be positive to obey the normalization requirement, $\int dR\, P(R) = 1$.

Only the small-size behavior of $P(R)$ affects the most interesting long time characteristics since in this regime only small particles can be adsorbed. Thus instead of (1) we shall use a power-law size distribution with an upper cutoff (taken as the unit of length):

$$P(R) = \begin{cases} \alpha\, R^{\alpha-1} & R \le 1; \\ 0 & R > 1. \end{cases} \qquad (2)$$

The patterns formed by PRSA are drastically different from traditional RSA patterns, since the coverage is complete for PRSA. The pore space of the patterns is a nontrivial fractal set. This is physically evident, and in one dimension it proves possible to determine the fractal

dimension $D_f(\alpha)$ analytically . In higher dimensions, we have to resort to numerical treatment.

Monte Carlo simulations of the PRSA model have been performed by implementing the following algorithm. A center of the new disc is chosen at random with a uniform probability density. The radius of the disc is generated according to the size-distribution of Eq. (2). If this disc does not overlap any other discs already in placed, it is deposited. Otherwise, the attempt is discarded. The maximal coverage studied in simulations was ~ 0.9 and about 100 runs were performed for each α. Some of the generated patterns are shown in Fig. 1. Clearly, the character of patterns changes when the exponent α increases from 0 to ∞. For the small α, the patterns look like a random set of little discs distributed uniformly over the plane, with larger discs randomly scattered in the "sea" of smaller ones. For large α, one recognizes a structure initially formed by large discs and then reproduced by smaller discs in the holes between the large ones. These properties of patterns follow from the small size behavior of radii distribution function $P(R)$. Indeed when $\alpha \to 0$ the smallest particles primarily participate in the adsorption, and hence apparently random patterns emerge. When $\alpha \to \infty$, the particles of the largest size are deposited until the system reaches the jamming limit of monodisperse RSA. Then the next particle to arrive will be the one that fits the biggest hole. This continues, so in this second stage the process is deterministic and apparently ordered patterns emerge.

On the length scales much smaller than the upper cutoff, patterns are self-similar (Fig. 2). This suggests the fractal nature of the arising patterns. We have measured the fractal dimension D_f of the pore-space of the patterns using the standard approach (see e.g. [15,16]) based on the analysis of the radii distribution function for the adsorbed particles. Namely, denote by $n(R)dR$ the number density of adsorbed discs with radii from the interval $(R, R+dR)$. Let ϵ is an arbitrary lower cutoff radius. Then $N(\epsilon) = \int_\epsilon^\infty dR\, n(R)$ gives the number density of discs with radii greater than ϵ. The power law behavior of $N(\epsilon)$ at the $\epsilon \to 0$ limit,

$$N(\epsilon) \sim \epsilon^{-D_f}, \tag{3}$$

is a signature that the pore space is a set of fractal dimension D_f. Numerically, we indeed observed this power law behavior. We also found that D_f monotonously decreases when α increases (see Fig. 3).

III. THEORETICAL APPROACHES TO PATTERN FORMATION

In the present section we employ scaling, mean-field and exact approaches to the process of pattern formation in PRSA. The first approach is based on the scaling hypothesis and gives relations between structural and kinetic characteristics of the system.

A. Scaling Framework

Let $\Phi(t)$ is the fraction of uncovered area and $\Psi(R,t)$ the probability that a disc of radius R can be placed onto a substrate [11]. Clearly,

$$\Psi(0,t) = \Phi(t). \tag{4}$$

$\Phi(t)$ evolves according to the *exact* rate equation

$$\frac{d\Phi}{dt} = -\int_0^\infty dR P(R)\Psi(R,t)V_d R^d, \tag{5}$$

where V_d denotes the volume of the d-dimensional unit sphere, $V_d = \pi^{d/2}/\Gamma(1+d/2)$. Assuming a scaling behavior of $\Psi(R,t)$, we write

$$\Psi(R,t) = S^\theta(t)\, F\left(\frac{R}{S(t)}\right). \tag{6}$$

Here $S(t) \sim t^{-\nu}$ is a typical gap between neighboring adsorbed particles and $F(x)$ is a scaling function. The scaling description applies when $t \to \infty$ and $R \to 0$ with $R/S(t)$ finite. The existence of scaling is an assumption, which is supported by numerical evidence in 2D and by analytical results in 1D [9].

Eqs. (4) and (6) imply $\Phi(t) \sim t^{-z}$ with $z = \theta\nu$. Substituting then (6) into (5) gives

$$\nu = \frac{1}{\alpha+d}, \quad z \simeq \alpha V_d \int_0^\infty dx\, x^{\alpha+d-1} F(x). \tag{7}$$

Scaling suggests that self-similar fractal structures should arise. Indeed, computing the number density of the absorbed particles we get

$$n(R) = \int_0^\infty dt\, P(R)\Psi(R,t) \sim R^{\alpha-1+(z-1)/\nu} \tag{8}$$

Hence, the power-law dependence of Eq. (3) is recovered when we identify the fractal dimension with

$$D_f = d - z(d+\alpha). \tag{9}$$

Eq. (9) provides a relation between the fractal dimension of the arising patterns and the kinetic exponent z. Similar qualitative behaviors were observed in other pattern formation models [16].

We should stress that scaling provides just a framework; for instance, it gives scaling relations among the exponents but it does not allow to compute the exponents. So one should use other approaches to get a complete exact or approximate description of PRSA. In one dimension, an exact description is indeed possible. In higher dimensions, even in the extreme case of $\alpha = \infty$ the fractal dimension of the pore space remains unknown, so analytical description of PRSA is hardly possible.

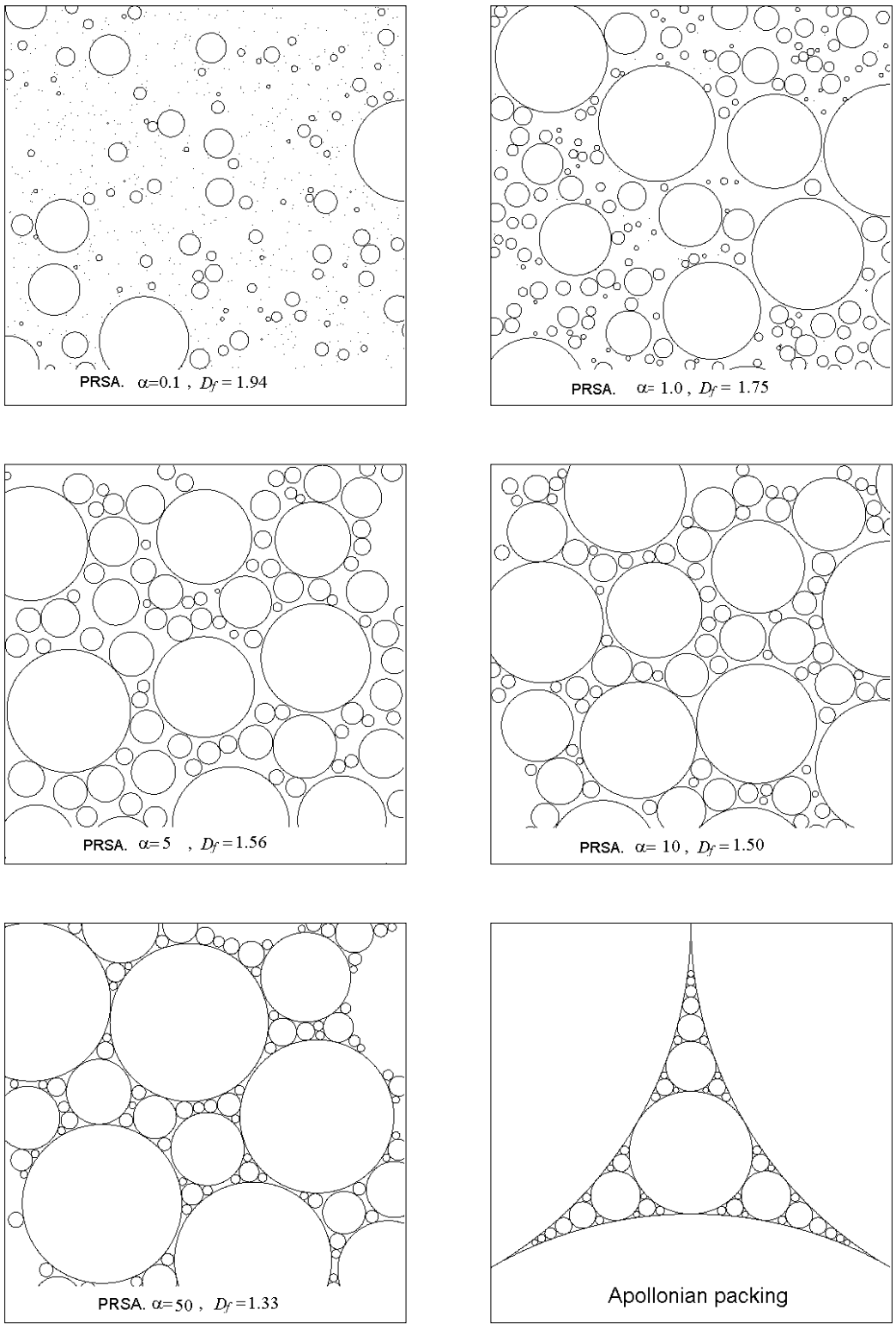

Fig. 1 Typical PRSA patterns for $\alpha = 0.1, 1, 5, 10, 50$ and Apollonian packing.

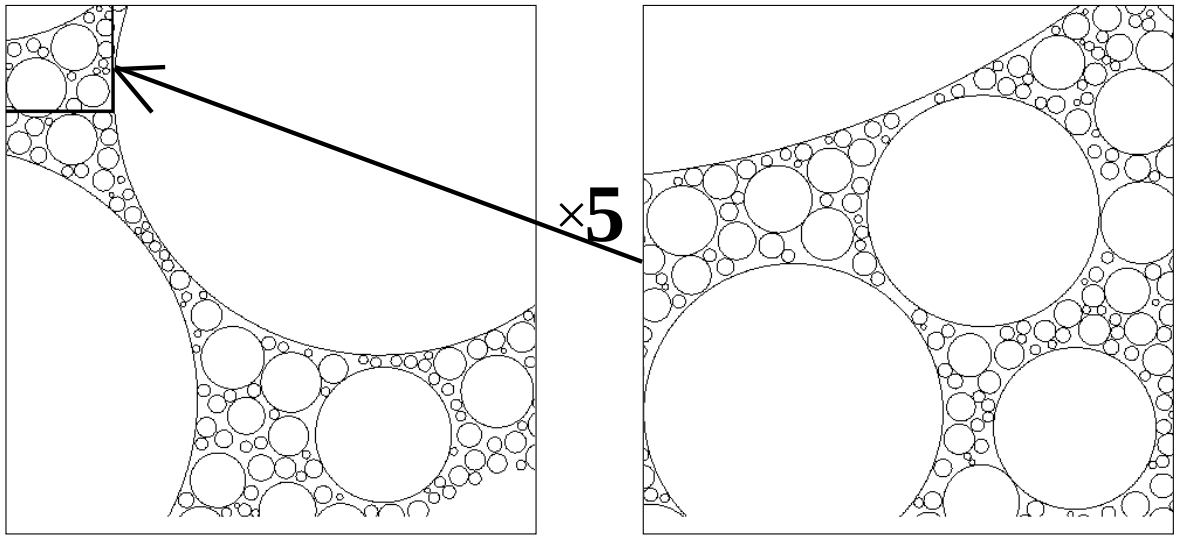

Fig. 2 Self-similarity of the PRSA patterns.

B. 1D PRSA: Exact Results

A detailed analysis of 1D PRSA is given in Ref. [9]. Here we sketch basic results which are necessary to determine the fractal dimension. Let $C(x,t)$ be the concentration of holes of length x at time t. All holes have the same "shape" in 1D that significantly simplifies the problem. By definition, $C(x,t)$ is related to $\Psi(x,t)$ via

$$\Psi(x,t) = \int_x^\infty dy(y-x)C(y,t). \tag{10}$$

The kinetic equation for $C(x,t)$ reads

$$\frac{\partial C(x,t)}{\partial t} = -C(x,t)\left[\int_0^x dz(x-z)P(z)\right] + 2\int_x^\infty dy\, C(y,t)\int_0^{y-x} dz\, P(z). \tag{11}$$

The first term on the right-hand side of Eq. (11) gives the loss of holes of length x due to deposition of intervals of length z (with $z < x$); the second term describes the gain of holes of length x from larger holes. Substituting $P(z) \equiv P(R)$ given by Eq. (2) into Eq. (11) yields

$$\left(\frac{\partial}{\partial t} + \frac{x^{\alpha+1}}{\alpha+1}\right) C(x,t) = 2\int_x^\infty dy\, C(y,t)(y-x)^\alpha. \tag{12}$$

Multiplying both sides of Eq. (12) by x^β and integrating over x gives the kinetic equation

$$\frac{dM_\beta}{dt} = \left[2\frac{\Gamma(\alpha+1)\Gamma(\beta+1)}{\Gamma(\alpha+\beta+2)} - \frac{1}{\alpha+1}\right] M_{\alpha+\beta+1} \tag{13}$$

for the moments of the hole-size distribution

$$M_\beta(t) = \int_0^\infty dx\, x^\beta C(x,t). \tag{14}$$

Eq. (10) implies $C(x,t) = \frac{\partial^2}{\partial x^2}\Psi(x,t)$. Combining this with the scaling ansatz of Eq. (6) we obtain

$$C(x,t) = S^{\theta-2}(t)\, F''\left(x/S(t)\right), \tag{15}$$

where $F''(\xi) = d^2F/d\xi^2$. Eq. (15) allows us to express the moments $M_\beta(t)$ via the time-independent moments,

$$M_\beta(t) = S^{\theta+\beta-1}(t) m_\beta, \quad m_\beta = \int_0^\infty d\xi\, \xi^\beta F''(\xi). \tag{16}$$

Choose now the exponent β so that the numerical factor on the right-hand side of Eq. (13) vanishes, i.e.,

$$2\frac{\Gamma(\alpha+1)\Gamma(\beta+1)}{\Gamma(\alpha+\beta+2)} = \frac{1}{\alpha+1}. \tag{17}$$

For such $\beta = \beta(\alpha)$, Eq. (13) implies that $M_\beta(t)$ does not depend on t. Eq. (16) therefore gives $\theta = 1-\beta$, and then other exponents and the fractal dimension are found:

$$\nu = \frac{1}{1+\alpha}, \qquad z = \frac{1-\beta}{1+\alpha}, \qquad D_f = \beta. \tag{18}$$

A simple analysis shows that (i) Eq. (17) has only one positive solution $\beta = \beta(\alpha)$, (ii) $\beta < 1$ for all $\alpha > 0$, and (iii) β decreases when α increases. One can determine $\beta = D_f$ explicitly in some specific cases, e.g., $D_f = (\sqrt{17} - 3)/2$ for the uniform size distribution ($\alpha = 1$).

C. Mean-Field Theory of PRSA

In higher dimensions we employ an approximate mean-field treatment. We shall use a mean-field description of PRSA close to the one developed in [16] for nucleation-and-growth processes. As usual, we shall ignore many-particles spatial correlations and account only two-particle ones. To find $\Psi(R,t)$, consider a circle of radius R centered at the origin. Then one can write the following estimate to this function in the mean-field spirit:

$$\Psi(R,t) = \exp\left\{-\int_0^t d\tau \int_0^R dr\, \Omega_d r^{d-1} \int_0^\infty d\rho\, P(\rho) \frac{\Psi(\rho,\tau)}{\Phi(\tau)}\right\} \quad (19)$$
$$\times \exp\left\{-\int_0^t d\tau \int_R^\infty dr\, \Omega_d r^{d-1} \int_{r-R}^\infty d\rho\, P(\rho) \frac{\Psi(\rho,\tau)}{\Phi(\tau)}\right\}.$$

The former exponential factor in (19) estimates the probability that our circle is not covered up to time t by discs with centers fall inside this circle. The latter exponential factor guarantees that the free space inside our circle is not covered by the other discs which were adsorbed outside the circle. We also denote by Ω_d the surface area of unit sphere in d dimensions, $\Omega_d = dV_d = 2\pi^{d/2}/\Gamma(d/2)$. The exponential factors in Eq. (19) were derived by noting that

$$d\tau\, dr\, d\rho\, \Omega_d r^{d-1} P(\rho)\Psi(\rho,\tau)$$

gives the probability that a disc of radius belonging to the interval $(\rho, \rho + d\rho)$ was adsorbed within the time interval $(\tau, \tau + d\tau)$ in the spherical shell centered at the origin and confined by radii r and $r + dr$. The factor $\Psi(\rho,\tau)$ guarantees that the disc of radius ρ may be placed into the system. Such event prevents the adsorption of disc of radius R at the origin. The probability that such event has not happened,

$$1 - d\tau\, dr\, d\rho\, \Omega_d r^{d-1} P(\rho)\Psi(\rho,\tau),$$

may be re-written as

$$\exp\left\{-d\tau\, dr\, d\rho\, \Omega_d r^{d-1} P(\rho)\Psi(\rho,\tau)\right\}.$$

The probability that none of these events has happened up to time t is obtained by multiplying all these factors with $0 \le \tau \le t$, $0 \le r \le \infty$, and $0 \le \rho \le \infty$. However one should take into account that above expression gives a correct estimate only for factors with $\tau = 0$. For subsequent factors with $\tau > 0$, one should use $\Psi(\rho,\tau)/\Phi(\tau)$ instead of $\Psi(\rho,\tau)$ since the preceding factors guarantee that the discs are placed on the uncovered space. Using $\Phi(0) = 1$ and treating separately $r \le R$ and $r \ge R$, one arrives at Eq. (19). Again we assume that in the scaling regime we can use Eq. (6) for the function $\Psi(R,t)$. Taking into account that $\Psi(0,t) = \Phi(t)$, we get

$$F(Rt^\nu) = \exp\left\{-\int_0^t d\tau \int_0^\infty d\rho\, \Omega_d P(\rho)\left((R+\rho)^d - \rho^d\right) F(\rho\tau^\nu)\right\}. \quad (20)$$

Remarkably, the ansatz

$$F(x) = \exp(-A_1 x - \ldots - A_d x^d) \quad (21)$$

reduces the nonlinear integral equation (20) to a system of d algebraic equations for coefficients A_j. In particular, in 1D we get $\nu = 1/(\alpha+1)$ and a closed equation for A_1:

$$A_1 = \frac{2\alpha}{1-\nu\alpha}\int_0^\infty dx\, x^{\alpha-1} e^{-A_1 x}. \quad (22)$$

Eq. (22) is solved to find $A_1 = [2\Gamma(\alpha+2)]^{\frac{1}{\alpha+1}}$. Thus on the mean-field level, the scaling function for 1D PRSA is pure exponential, i.e. it is clearly different from the analytical solution. To obtain a quantitative difference we substitute $F = e^{-A_1 x}$ with the above value of A_1 into Eq. (7) to find $z = \frac{\alpha}{\alpha+1}$. Substituting this into Eq. (9) we obtain the fractal dimension: $D_f^{\rm MF} = 1 - \alpha$ for $\alpha < 1$ and $D_f^{\rm MF} = 0$ for $\alpha \ge 1$. Thus the mean-field theory is clearly wrong for $\alpha \ge 1$, though in the limit $\alpha \to 0$ it becomes exact [17]. For instance, $D_f^{\rm exact} - D_f^{\rm MF} = (\frac{2\pi}{3} + 4\gamma^2 - 2 - 6\gamma)\alpha^2 + \mathcal{O}(\alpha^3)$ (here $\gamma \cong 0.57721566$ is the Euler constant).

For 2D PRSA, the ansatz of Eq. (21) yields

$$A_1 = 2\pi\alpha(\alpha+2)\int_0^\infty dx\, x^\alpha e^{-A_1 x - A_2 x^2},$$
$$A_2 = \frac{\pi}{2}\alpha(\alpha+2)\int_0^\infty dx\, x^{\alpha-1} e^{-A_1 x - A_2 x^2}.$$

Solving these equations numerically, and then inserting $F(x) = e^{-A_1 x - A_2 x^2}$ into Eq. (7), one finds z and D_f.

In the small α limit, we perform a perturbation analysis to find [18]

$$A_1 = 2\pi\alpha + a_1\alpha^2 = 2\pi\alpha - 17.3557\alpha^2,$$
$$A_2 = \pi + a_2\alpha + a_3\alpha^2 = \pi - 1.8339\alpha + 12.6546\alpha^2,$$

where we have omitted terms of order $\mathcal{O}(\alpha^3)$. Using these expressions for A_1 and A_2, we get the kinetic exponent

$$z = \alpha/2 + a_4\alpha^2 = \alpha/2 - 1.5428\alpha^2 + \cdots \quad (23)$$

and for the fractal dimension

$$D_f = 2 - \alpha + a_5\alpha^2 = 2 - \alpha + 2.5856\alpha^2 + \cdots. \quad (24)$$

The mean-field predictions for $D_f(\alpha)$ and $z(\alpha)$ are shown on Fig. 3 and Fig. 4. We see that the mean-field approach provides a fair description for small α. For $\alpha \simeq 1$, however, the spatial correlations become more and more important and the mean-field theory fails.

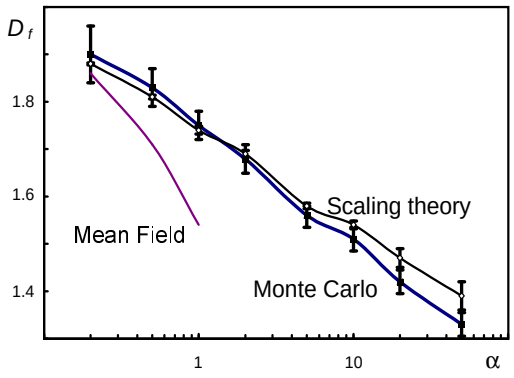

Fig.3 The fractal dimension D_f vs. α in two dimensions. D_f of the scaling theory is obtained from Eq. (9) with the "experimental" value of the kinetic exponent z.

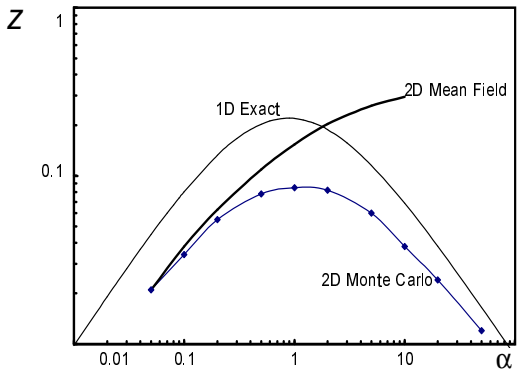

Fig.4 The kinetic exponent z vs. α in one and two dimensions.

D. The Limit $\alpha \to \infty$

When $\alpha = \infty$, the PRSA process develops through two stages. The initial stage is just RSA of monodisperse particles of radii $R = R_{\max} = 1$. It continues until the jamming coverage, $\Phi_\infty \cong 0.542$, is reached. Then the late stage begins, where the next disc to place would be the one that fits the biggest hole. The dynamics in this late stage is thus deterministic and extremal. This deterministic procedure has been applied by Apollonius of Perga 200BC to fill the space between three "kissing" discs [12]. In the present case, the procedure fills uncovered space obtained during the initial RSA stage. As the process develops, new discs will be placed more and more often into the curvilinear triangles confined by three kissing discs. Such curvilinear triangles are filled independently, so locally our packing should be identical to Apollonian packing. The fractal dimension quantifies local characteristics of the pattern, so we conclude that $D_f(\infty) = D_A$.

The fractal dimension of Apollonian packing is $D_A \cong 1.3057$ in two dimensions. Note that the fractal dimension of the Apollonian parking, arguably the oldest known fractal, has not been computed analytically in higher dimensions, so the exact value of $D_f(\infty) = D_A$ remains unknown. The only trivial exception is the one-dimensional case where the holes remaining after the initial stage are filled up completely during the deterministic stage. The number density $n(x) \equiv C(x, t = \infty)$ of adsorbed intervals of length x is [19]

$$n(x) = 2\int_0^\infty dt\, t \exp\left[-xt - 2\int_0^t d\tau \frac{1-e^{-\tau}}{\tau}\right]. \quad (25)$$

$n(x)$ exhibits a weak integrable singularity in the small size limit, $n(x) \sim \ln(1/x)$, implying that $N(\epsilon)$ is regular and therefore $D_f(\infty) = 0$ [20]. This agrees with previous exact results, Eqs.(17) and (18), which provide the asymptotic behavior $D_f(\alpha) \simeq \frac{\ln 2}{\ln(\alpha+2)}$ when $\alpha \to \infty$.

IV. ORDERING IN THE RSA

For a quantitative description of the ordering processes we introduce an entropy, S_N, characterizing the degree of order of N-particle patterns. Let C denotes a particular N-particle pattern and $p_N(C)$ denotes the probability of that pattern. We can define the Shannon entropy [21,22]:

$$S_N = -\sum_C p_N(C) \log_2 p_N(C) \quad (26)$$

As it follows from Eq. (26), $S_N = 0$ for a regular pattern, since only one configuration (which occurs with the probability $p_N = 1$) contributes to the entropy. A closely related quantity, $dS_N/dN \simeq S_{N+1} - S_N$, gives the entropy production rate per particle and characterizes the regularity of the pattern formation process. We also introduce the conditional entropy, $S^*_{N+1}(C)$, characterizing patterns built by adding a disc to a given N-particle pattern C:

$$S^*_{N+1}(C) = -\sum_{R,\vec{r}} p(R,\vec{r}|C) \log_2 p(R,\vec{r}|C). \quad (27)$$

Here $p\,(R,\vec{r}|C)$ is the conditional probability to add a disk of radius R at point $\vec{r}$ to the particular pattern $C(N)$ of N disks. The total probability of the $N+1$-particle configuration, obtained from the pattern C by placing an additional disc, reads:

$$p_{N+1}(R,\vec{r},C) = p(R,\vec{r}|C)p_N(C). \quad (28)$$

S_{N+1} can be written as

$$S_{N+1} = -\sum_{R,\vec{r},C} p_{N+1}(R,\vec{r},C) \log_2 p_{N+1}(R,\vec{r},C). \quad (29)$$

Using Eqs. (26)–(29) and the normalization condition, $\sum_{R,\vec{r}} p(R,\vec{r}|C) = 1$, we finally arrive at the entropy production rate:

$$\frac{dS_N}{dN} \simeq S_{N+1} - S_N = \sum_C p_N(C) S^*_{N+1}(C). \qquad (30)$$

Thus the entropy production rate is obtained by averaging the conditional entropy over all possible configurations.

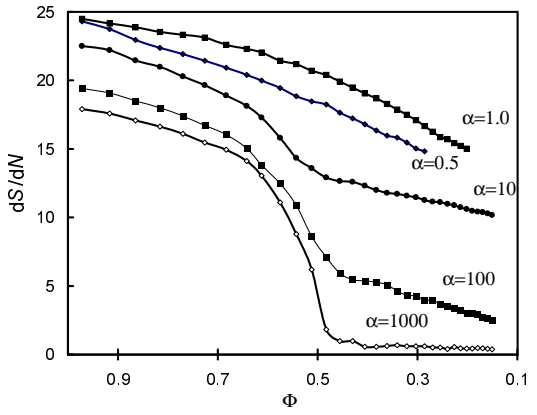

Fig.5 The entropy production rate vs. the uncovered area for different values of α. A sharp decay at $\Phi \approx 0.55$ is clearly seen for large α.

In spite of apparent simplicity of the definition of the entropy production rate, its analytical evaluation is a very challenging problem even in one dimension. Indeed, it requires knowledge of the multiparticle probability distribution function. In the simplest case of the monodisperse RSA we do know the first two moments of $p(C)$, the density [5] and the pair correlation function [23], but much more detail information is needed for determination of the entropy production rate. Thus we investigated this quantity numerically for 2D system by means of Monte Carlo simulations. We implemented the following algorithm. A disc which is added to the pattern $C(N)$ of N disks was treated as a point in a the "configurational" space $(R,\vec{r}) = (R,x,y)$. We divided the continuous configuration space into sufficiently small discrete cells and enumerated these cells. For computations we used cells of linear size 0.01 and 5×5 fragment of the surface (with $R_{max} = 1$, see (2)); thus, the total number of cells was $M = 2.5 \times 10^7$. Then the conditional probabilities, $p\,(R,\vec{r}|C(N)) = p_i$, that $(N+1)$-th disk comes to the $i^{\rm th}$ cell, corresponding to $(R,\vec{r})$ in the given configuration, $C(N)$, of N discs was calculated numerically from

$$p_i = \frac{A_i R_i^{\alpha-1}}{\sum_{j=1}^{M} A_j R_j^{\alpha-1}} \qquad (31)$$

where $A_i = 0$ if the disc corresponding to the $i^{\rm th}$ cell overlaps with some disc in the pattern $C(N)$; otherwise, $A_i = 1$. Eq. (31) follows from the rate of adsorption, (2), and the normalization condition for the probability. The discrete conditional probabilities (31) are used to calculate the conditional entropy $S^*_{N+1}(C)$ via Eq. (27). Finally, the entropy production rate was obtained by averaging $S^*_{N+1}(C)$ over C according to Eq. (30). The averaging was performed over 10^2 Monte Carlo runs, and the accuracy of the method was controlled through run-to-run deviations.

To compare the entropy production rate for different values of α, we plot dS_N/dN versus Φ (see Fig. 5). The striking behavior of the entropy production rate is clearly seen in the large α limit: At the beginning of the process of pattern formation (i.e., when $\Phi \approx 1$), the entropy production rate decreases slowly similar to the small α case. Around $\Phi \approx 0.55$, however, a sharp decay occurs. The threshold value, $\Phi \approx 0.55$, is close to the jamming density, $\Phi_\infty \cong 0.542$, of the RSA of identical discs. The transition demarcates the initial random stage when discs of maximal radii are deposited and the final deterministic stage when discs of maximal possible radius are inserted into maximal holes. Given the deterministic nature of the final stage, the entropy production rate should be equal to zero when $\alpha = \infty$ and $\Phi \geq \Phi_\infty$. This is in agreement with our numerical findings for large α.

V. SUMMARY

In summary, we investigated the adsorption kinetics and spatial properties of the arising patterns in RSA of polydisperse particles whose size distribution has a power-law form in the small size limit. We developed a scaling approach and verified that it indeed applies by comparing with exact results in one dimension and numerical results in two dimensions. We found that arising patterns are self-similar fractals that appear to be completely random when deposited particles are predominantly small; in the opposite limit highly ordered structures, locally isomorphic to Apollonian parking, are formed. The fractal dimension D_f of the pore space is determined by the power-law exponent α of the particles size distribution. When α increases from 0 to ∞, D_f decreases from 2 to $D_A \cong 1.305$, of the Apollonian packing. We introduced the entropy production rate as a quantitative measure of the regularity of arising patterns. We observed that for sufficiently small α, the entropy production rate smoothly decays as the coverage increases. In the complimentary case of $\alpha \gg 1$, the entropy production rate displays a similar behavior for sufficiently small coverage, followed by a sharp decay to a very low entropy production rate. Physically, it reflects a two-stage nature of the pattern formation process in the large α

limit: The ordinary RSA, that goes until the jammed state is reached, leads to a random structure which is starting point for the second stage. During this late stage the deposition process is deterministic and extremal – at a given step, the largest hole is filled.

One of us (PLK) acknowledges NSF grant DMR-9632059 and ARO grant DAAH04-96-1-0114 for financial support.

---

[1] P. J. Flory, *J. Amer. Chem. Soc.* **61**, 1518 (1939).

[2] J. Feder and I. Giaever, *J. Colloid Interface Sci.* **78**, 144 (1980); A. Yokoyama, K. R. Srinivasan, and H. S. Fogler, *J. Colloid Interface Sci.* **126**, 141 (1988).

[3] E. S. Hood, B. H. Toby, and W. H. Weinberg, *Phys. Rev. Lett.* **55**, 2437 (1985).

[4] J. D. Weeks and G. H. Gilmer, *Adv. Chem. Phys.* **40**, 157 (1979).

[5] M. C. Bartelt and V. Privman, *Int. J. Mod. Phys.* **5**, 2883 (1991); J. W. Evans, *Rev. Mod. Phys.* **65**, 1281 (1993); J. J. Ramsden, *J. Stat. Phys.* **79**, 491 (1995).

[6] G. S. Baker and M. J. Grimson, *Mol. Phys.* **63**, 145 (1987).

[7] J. Talbot and P. Schaaf, *Phys. Rev. A* **40**, 422 (1989).

[8] P. Meakin and R. Jullien, *Physica A* **187**, 475 (1992).

[9] P. L. Krapivsky, *J. Stat. Phys.* **69**, 135 (1992).

[10] W. Soppe, *Powder Technology* **62**, 189 (1990); N. Standish, A. B. Yu, and R. P. Zou, *Powder Technology* **68**, 175 (1991).

[11] A preliminary account of this work has been reported in N. V. Brilliantov, Yu. A. Andrienko, P. L. Krapivsky, and J. Kurths, *Phys. Rev. Lett.* **76**, 4058 (1996).

[12] B. B. Mandelbrot, *The Fractal Geometry of Nature* (San Francisco, Freeman, 1982).

[13] J. F. Douglas, H. M. Schneider, P. Frantz, R. Lipman, and S. Granick, *J. Phys. Condens. Matter* **9**, 7699 (1997).

[14] G. V. Schulz, *Z. Phys. Chem. Abt.* **43**, 25 (1939).

[15] S. S. Manna and H. J. Herrmann, *J. Phys. A* **24**, L481 (1991).

[16] Yu. A. Andrienko, N. V. Brilliantov, and P. L. Krapivsky, *J. Stat. Phys.* **75**, 507 (1994); N. V. Brilliantov, P. L. Krapivsky, and Yu. A. Andrienko, *J. Phys. A* **27**, L381 (1994).

[17] It was rigorously shown in [9] that for $\alpha \to 0$, the concentration of holes in the scaling limit, $y \to 0$, $t \to \infty$, behaves as $C(y,t) \sim t^2 \exp(-yt)$, i.e. the scaling function is exponential as in the mean-field theory.

[18] $a_1 = \frac{\pi^2}{6} - \frac{37\pi}{12} + \frac{\pi^2 b_1}{3} - 4\pi b_0$; $\quad a_2 = \frac{\pi}{12} - \frac{\pi^2}{6}\,(1 + 2b_1)$; $a_3 = \frac{19\pi^2}{12} - \frac{5a_2^2}{6\pi} - \frac{5a_2}{12} - 2\pi b_0 - b_1\left(2a_2 + 2\pi a_2 b_3 - \frac{7\pi}{2}\right)$; $a_4 = 2\pi b_1 + \pi + \frac{a_2}{2} - \frac{1}{2}$; $\quad a_5 = \pi - \frac{1}{2} + \frac{a_2}{2} + 2\pi b_1$. The constants b_k are given by $b_k = \int_0^\infty dx\, x^k \ln x\, e^{-\pi x^2}$ and may be expressed via gamma and digamma functions: $b_k = \frac{1}{4}\,\Gamma(\frac{k+1}{2})\,\pi^{-(k+1)/2}\left[\psi(\frac{k+1}{2}) - \ln\pi\right]$.

[19] $C(x,t)$ for $\alpha \to \infty$ is given, e.g., in [9].

[20] In 1D, the appropriate version of Apollonian construction is trivial and has $D_A = 0$. One can define artificial versions with finite fractal dimension, see e.g. M. K. Hassan, *Phys. Rev. E* **55**, 5302 (1997).

[21] M. C. Mackey, *Rev. Mod. Phys.* **61**, 981 (1989).

[22] The summation over a continuous set of configurations implicitly assumes that we consider a finite subset of configurations; in a numerical implementation, this is clearly the case.

[23] B. Bonnier, D. Boyer, and P. Viot, *J. Phys. A* **27**, 3671 (1994).